A new tool based on artificial neural networks for the design of lightweight ceramic–metal armour against high-velocity impact of solids

D. Fernández-Fdz *, R. Zaera

Department of Continuum Mechanics and Structural Analysis, University Carlos III of Madrid, Avda. de la Universidad, 30, 28911 Leganés, Madrid, Spain

A B S T R A C T

A new tool based on artificial neural networks (ANNs) has been developed for the design of lightweight ceramic metal armours against high velocity impact of solids. The tool developed predicts, in real time, the response of the armour: impacting body arrest or target perforation are determined and, in the latter case, the residual mass and velocity of the impacting body are determined. A large set of impact cases has been generated, by FEM numerical simulation, in order to train and test the ANN. The impact cases consider different impacting body and target geometries, materials and impact velocities, all these parameters varying in a wide range that covers most common impact situations. The behaviour of the ceramic material under impact was simulated using a modified version of the model developed by Cortés et al. The ANN developed has a remarkable prediction ability and therefore it constitutes a complementary methodology to the conventional design techniques.

1. Introduction

Armour design focuses on its protective capacity, cost, and areal density (weight/area), the relative importance of these requirements depending on the characteristics of the system to be protected. In the case of defensive walls or bunkers, weight is not a determining factor and low-cost materials can be used, increasing the resistance with larger thicknesses. However, weight is a key factor in the design of materials for protection against impact for moving objects – vehicles, civil or military aircraft, and personnel of security and defense corps. In land vehicles, a light protective armour allows the use of a lower-powered engine without sacrificing speed or maneuverability of the vehicle. In aircraft, the weight of each component must be considered, including the density of the armour plating. This is extremely important in protecting personnel whose mobility is essential. Various materials can be used to fulfil the requirements of a protection. Metals are generally adequate and their cost is reasonable, but their high density is a drawback. The use of ceramic materials is limited by their fragility, as they shatter on account of their poor toughness. Thus, the combination of the light weight and high hardness of the ceramics with the ductility of metals in the so-called mixed protections provides ballistic efficiency against the impact of low and medium caliber projectiles, and made great headway at the end of the 1960s (Florence, 1969). This type of protection, 60% lighter than the steel armours, is composed of a tile of ceramic material that receives the impact, and a metal backplate. The two components are normally joined by a thin layer of adhesive. The hard ceramic material is meant to erode the head of the projectile while the metal plate withstands the fragments of the ceramic and absorbs the kinetic energy of the projectile during its penetration. The protection can be used alone, to arrest the projectile, or it can serve as an additional protection over a backing armour.

* Corresponding author. Tel.: +34 916248809; fax: +34 916249973.
E mail address: dfernand@ing.uc3m.es (D. Fernández Fdz).

The design of lightweight ceramic–metal armours is a complex task for which three different methodologies are traditionally followed: experimental testing, numerical simulation and analytical modelling. The experimental method is widely used. It provides the highest accuracy but has the disadvantage of being valid exclusively for the particular projectile-target system at hand. It is also costly, requiring expensive installations (shooting galleries) and equipment (powder or gas guns, high-speed cameras) (Chocron Benloulo and Sánchez-Gálvez, 1998; Shokrieh and Javadpour, 2008). Semi-empirical techniques are often developed in parallel in order to extend the validity of real-fire tests to other projectile-target configurations, by the matching of the experimental results and extrapolating the results to other systems (Hetherington, 1994; Hohler et al., 2001).

The need for designing tools to be used as an alternative or complement to the experimental tests prompted the development of different simulation methodologies. Thus, the use of firing trials has been relegated to the final stage of the design. Numerical modelling provides a full solution of the penetration process by solving the whole set of differential equations of the thermomechanics of continuous media, leading to reliable results. The broader information provided by finite element or meshless codes (Wilkins, 1978; Cottrell et al., 2003) enables a better understanding of the process and is quite valuable for an improved design of the armour. However, to be able to use the codes and interpret the results, the worker needs a high degree of training. The relatively long CPU time required for a single simulation is another shortcoming of this approach as an armour design tool.

The third approach is the development of simplified analytical models (Den Reijer, 1991; Zaera and Sánchez-Gálvez, 1998) that represent the impact process by straightforward equations, assuming some hypotheses which simplify the actual mechanisms of the penetration process. Material description is simplified by using a few material parameters easily determined by experimentation. The main advantage of this approach is that it provides the solution of a definite projectile-target system in a few seconds with a personal computer. Quick and easy to use, this system allows the simulation of a large number of impact problems in the early stages of design, limiting the number of materials and the thicknesses to be considered. This saves substantial time and money that would be spent if the earlier methods were used. Disadvantages involve the lower accuracy of such models compared to full numerical simulation. Also the strong hypothesis considered for their development lead to simulation tools of limited versatility, each model having a specific application range. Therefore a design engineer needs a low-cost tool that would not only enable him to solve a problem of impact in the shortest possible time, but would also be easy to use and would give the required precision for a broad range of projectile/armour configurations. These features are specially desirable in the initial stages of design.

In the current multidisciplinary framework of engineering, with the vast increase in artificial computation techniques, neural networks are providing low-cost solutions to mechanical problems that are characterized by: (1) a high nonlinearity, (2) a dependence on a high number of parameters and (3) a wide range of variation of these parameters. These characteristics certainly apply to high-velocity impact on lightweight armours. Multilayer perceptron (MLP) is the most commonly applied neural network in the field of mechanics. MLP has been applied to solve a wide range of problems ever since the first work was published in Civil Engineering in 1989 (Adeli and Yeh, 1989). This network has been used to solve such problems as the bending of elastoplastic beams, damage detection in steel beams, or estimation of vibrations in buildings (Waszczyszyn and Ziemianski, 2001). Ince (2004) has applied a MLP to determine fracture parameters in concrete and Liu et al. (2002) have developed a non-destructive testing tool based on a MLP for crack detection. In this sense, composite materials have been amply studied, above all in damage detection but also in the characterization of its mechanical behaviour (see the complete review by El Kadi (2006)). In the framework of the constitutive equations, Waszczyszyn and Pabisek (1999) have integrated a MLP in a finite element code to update the stress in 2D elastoplastic problems. More recently, focussing on the field of *impact mechanics*, Remennikov and Rose (2007) have developed a predictive tool based on a MLP to determine the behaviour of blast-wall barriers, and Chandrashekhara et al. (1998) have studied the contact force for low-velocity impacts on laminated composite plates. It is also important, the work presented by Liu et al. (2003), where a backpropagation neural network is used in combination with a conjugate gradient method to optimize de design of metal/ceramic functionally graded materials armours.

This paper presents a tool, based on artificial neural networks, to analyse the response of ceramic–metal armours against high-velocity impact of projectiles. The network shows a remarkable ability to predict arrest of the projectile or perforation and, in the latter case, its residual mass and velocity.

2. Multilayer perceptron approach

2.1. The artificial neuron

In feedforward networks, such as MLP, a processing element or artificial neuron (Fig. 1a) receives outputs x_j from neurons of the previous layer which are weighted by synapse weights φ_{ji}. Neuron activation occurs when the sum of these weighted signals exceeds a pre-set value known as threshold activation, b_i. If the neuron is fired, it generates an output v_i, determined by the expression

$$v_i = f_i\left(\sum_{j\ 1}^{k} \varphi_{ji} x_j \quad b_i\right), \tag{1}$$

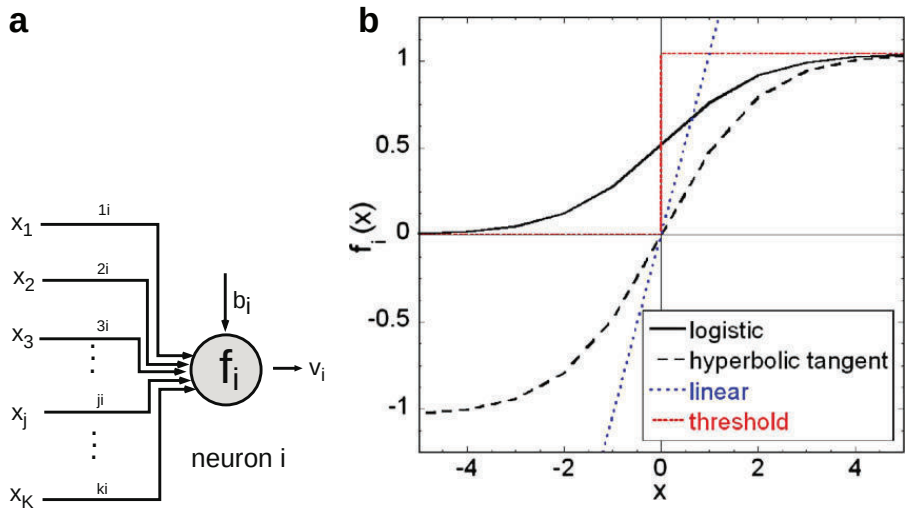

Fig. 1. (a) Computational model of the artificial neuron. (b) Some common activation functions f_i: logistic, hyperbolic tangent, linear and threshold.

f_i being the activation function. Some examples of functions f_i are shown in Fig. 1b.

2.2. Topology of the multilayer perceptron

The topology of a MLP (Fig. 2) is characterized by grouping neurons in the input, hidden, and output layers. In the input layer the identity function is used (linear with slope equal to one). In the hidden and the output layer, logistic, threshold and hyperbolic tangent functions can be employed. This network presents total connectivity, which means that each neuron is connected to all the neurons of contiguous layers but not with those located in the same layer. Unlike other topologies such as recurrent neural networks, connections are made from the input to the output layer, mapping a N-component vector $\mathbf{x}$ containing the input variables in a M-component vector $\mathbf{y}$ containing the output variables, so that a MLP defines a nonlinear continuous function $\mathscr{F}$ from R^N to R^M

$$\mathbf{y} = \mathscr{F}(\mathbf{x}, \Phi, \beta). \tag{2}$$

Φ and β being the set of weights φ_{ji} and thresholds b_i. These values are adjusted during the training stage to minimize the error when the MLP produces an output $\mathbf{y}$ corresponding to an input $\mathbf{x}$.

2.3. Training algorithm of the multilayer perceptron

The patterns $(\mathbf{x}, \mathbf{y})_s$ form the variability space $\mathscr{R}$ of the excitation and response of the system studied (Fig. 3a). During the training process the MLP extracts the characteristics of the system from a reduced set of training patterns $\mathscr{K}$ in which both inputs and outputs are known

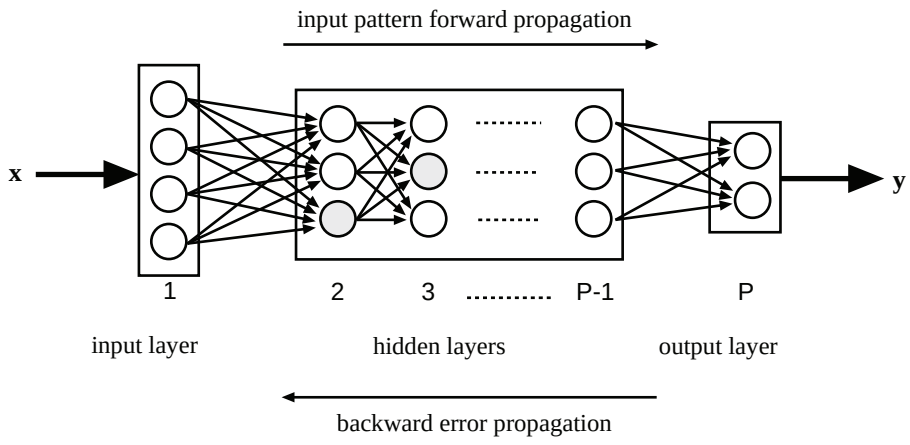

Fig. 2. Multilayer perceptron topology: feedforward network with backward propagation error and P layers (1 input layer, 1 output layer and P 2 hidden layers).

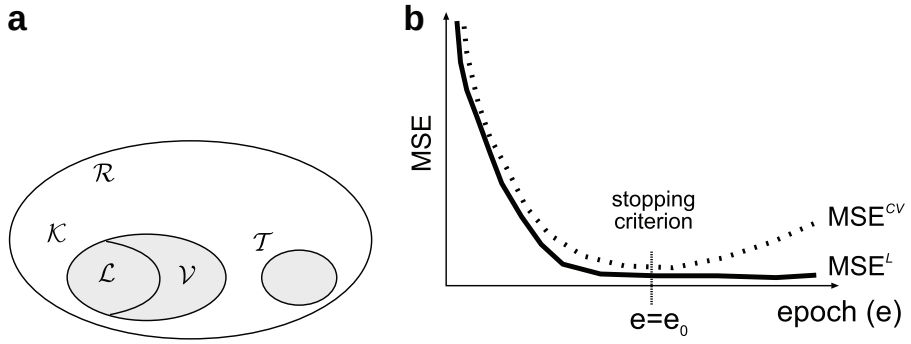

Fig. 3. (a) Variability space $\mathscr{R}$ of $(\mathbf{x},\mathbf{y})$: sets of training ($\mathscr{K}$), testing ($\mathscr{T}$), learning ($\mathscr{L}$) and cross validation ($\mathscr{V}$) patterns. (b) MSE vs. iteration number (epoch) for learning and cross validation.

$$\mathscr{K} = \{(\mathbf{x},\mathbf{y})_s^{\mathscr{K}} | s = 1,\ldots,K\} \subset \mathscr{R}, \tag{3}$$

which is randomly divided in the subset of learning $\mathscr{L}$ and the subset of cross-validation $\mathscr{V}$:

$$\mathscr{L} = \{(\mathbf{x},\mathbf{y})_s^{\mathscr{L}} | s = 1,\ldots,L\} \subset \mathscr{K}, \tag{4}$$

$$\mathscr{V} = \{(\mathbf{x},\mathbf{y})_s^{\mathscr{V}} | s = 1,\ldots,V\} \subset \mathscr{K}. \tag{5}$$

The first set is used to determine the values of Φ and β through the backpropagation algorithm or generalized delta rule proposed originally by Rumelhart et al. (1986). The algorithm iteratively modifies the initial values of weights and thresholds to arrive at the minimum value of a function which measures the predictive error of the network, following the direction of the gradient descent of this function. Although there are many definitions of the error, the most common one is the mean squared one

$$\text{MSE} = \frac{1}{K}\sum_{s\ 1}^{K} \mathbf{e}(s,\Phi,\beta), \tag{6}$$

$\mathbf{e}(s,\Phi,\beta)$ being the squared error for a pattern s:

$$\mathbf{e}(s,\Phi,\beta) = \frac{1}{2}\sum_{i\ 1}^{\mathrm{M}} (y_{\mathrm{i}}^*(s) \quad y_{\mathrm{i}}(s,\Phi,\beta))^2, \tag{7}$$

where $y_{\mathrm{i}}^*(s)$ is the desired output for parameter i and $y_{\mathrm{i}}(s,\Phi,\beta)$ is the predicted output for parameter i, that is defined, by applying expression (1), as

$$y_{\mathrm{i}}(s,\Phi,\beta) = v_{\mathrm{i}}^P(s,\Phi,\beta) = f_i^P\left(\sum_{j\ 1}^{k_P} \varphi_{ji}^{P-1} v_j^{P-1} \quad b_i^P\right), \tag{8}$$

so the squared error is written as a function of s, Φ and β:

$$\mathbf{e}(s,\Phi,\beta) = \frac{1}{2}\sum_{i\ 1}^{\mathrm{M}} \left(y_{\mathrm{i}}^*(s) \quad f_i^P\left(\sum_{j\ 1}^{k_P} \varphi_{ji}^{P-1} v_j^{P-1} \quad b_i^P\right)\right)^2. \tag{9}$$

A commonly adopted procedure to correct the values of Φ and β is the stochastic gradient descent, which uses the error of a pattern $\mathbf{e}(s)$, instead of a global measure of the error, according to the expressions

$$\begin{aligned} \varphi_{ji}^{p-1}(s+1) &= \varphi_{ji}^{p-1}(s) \quad \xi\frac{\partial \mathbf{e}(s)}{\partial \varphi_{ji}^{p-1}}, \\ b_i^p(s+1) &= b_i^p(s) \quad \xi\frac{\partial \mathbf{e}(s)}{\partial b_i^P} \end{aligned} \tag{10}$$

ξ being the learning rate. The derivatives in Eq. (10) are calculated using the generalized delta rule (Rumelhart et al., 1986). The training process can be summarized as follows:

- Weights and thresholds are randomly initialized with values close to zero.
- The input $\mathbf{x}^{\mathscr{L}}(1)$ (from first learning pattern) is propagated, an output $\mathbf{y}(1)$ is determined, and error $\mathbf{e}(1)$ is computed.
- The backpropagation algorithm is applied and weights and thresholds are incremented in the negative direction of the error gradient.

- The two previous steps are repeated for the rest of the learning patterns $(\mathbf{x},\mathbf{y})_s^{\mathscr{L}}$, updating Φ and β each time.
- The global learning error $\mathrm{MSE}^{\mathscr{L}}$ is computed and an epoch (learning cycle) is completed.
- Consecutive epochs are repeated until a stable value of $\mathrm{MSE}^{\mathscr{L}}$ is reached (Fig. 3b).

The cross-validation subset $\mathscr{V}$ of training patterns is used during the application of the backpropagation algorithm to prevent *overlearning* of the MLP. This spurious effect consists of an accurate prediction of the output belonging to the patterns of the learning subset $\mathscr{L}$ but not for independent inputs. Thus, the cross-validation global error $\mathrm{MSE}^{\mathscr{V}}$ is calculated at the end of each epoch and the learning algorithm is stopped when this error starts to increase (Fig. 3b). Once the training algorithm has finished, the testing set $\mathscr{T}$:

$$\mathscr{T} = \{(\mathbf{x},\mathbf{y})_s^{\mathscr{T}} | s = 1,\ldots,T\} \subset \mathscr{R} \tag{11}$$

is used to check the predictive ability of the MLP with patterns independent from those employed during training. If the error associated to the test results is below that demanded by the application requirements, the network is ready to generate reliable output data.

3. Data collection: impact cases generation

Having a training set $(\mathscr{K})$ and a testing set $(\mathscr{T})$ broad enough to cover a representative part of the variability space $\mathscr{R}$ of the patterns $(\mathbf{x},\mathbf{y})$ – the impact cases – is one of the main difficulties of this work. In consideration of the discussion in Section 1, the experimental method and the analytical modelling have been rejected due to the difficulties associated with the former and the limitations of the latter. Therefore, numerical simulation has been employed to generate these sets of patterns. No precise guidelines exist to determine the number n of patterns necessary to train the network. This number can be bounded by the expression given by Tarassenko (1998)

$$N_{\phi\beta} < n < 10N_{\phi\beta}, \tag{12}$$

where $N_{\phi\beta}$ is the number of fitting parameters of the network (thresholds and weights). Although the impact of a projectile onto a ceramic/metal target is a highly non-linear problem, slight variations of an input parameter do not lead to sharp variation of the outputs and its effect is monotonous (i.e., an increase in the target thickness always reduces the residual velocity). Therefore, the number of cases considered for training was closer to the lower limit proposed by Tarassenko. A preliminary analysis of the neurons required to solve this problem (eight for input, four for output and eight for hidden) leads to 116 fitting parameters, so we have generated and simulated 200 impact cases, of which 185 will be employed for training and 15 for testing, having $n \simeq 1.5N_{\phi\beta}$.

The problem of high velocity normal impact of cylindrical projectiles on lightweight ceramic–metal armours can be defined by the following variables:

(1) Projectile length (L_p).
(2) Projectile diameter (D_p).
(3) Impact velocity (v_i).
(4) Ceramic tile thickness (H_c).
(5) Metal plate thickness (H_m).
(6) Projectile material.
(7) Ceramic tile material.
(8) Metal plate material.

The input pattern $\mathbf{x}$ can be formed by these or a combination of them. Two different materials have been used for the projectile (tungsten and high-strength steel), for the ceramic tile (alumina and aluminium nitride) and for the metal plate (aluminium and mild steel). A wide variation range for quantitative parameters has been established to cover most cases of the high-velocity impact with low and medium caliber projectiles:

$$\begin{aligned} &4\ \mathrm{mm} \leqslant D_\mathrm{p} \leqslant 12\ \mathrm{mm},\\ &3 \leqslant L_\mathrm{p}/D_\mathrm{p} \leqslant 6,\\ &0.3 \leqslant (H_\mathrm{c}+H_\mathrm{m})/L_\mathrm{p} \leqslant 0.6,\\ &1 \leqslant H_\mathrm{c}/H_\mathrm{m} \leqslant 3,\\ &500\ \mathrm{m/s} \leqslant v_\mathrm{i} \leqslant 1200\ \mathrm{m/s}. \end{aligned} \tag{13}$$

The values of these parameters have been determined following a uniform distribution of probability. The impact cases generated with these restrictions have been created following a random sampling.

In armour design, for an armour/projectile system, is useful to determine the ballistic limit v_{50} (the minimum velocity at which a particular projectile is expected to completely penetrate an armour of given thickness and physical properties with a 50% of probability). In case of perforation, is also useful to determine the residual mass and residual velocity of the projectile.

These latter two variables enable the evaluation of the residual kinetic energy of the projectile. Thus the output pattern **y**, determined by numerical modelling, is formed by the variables:

- Occurrence of target perforation.
- Residual velocity of the projectile v_r (in case of perforation).
- Residual mass of the projectile m_r (in case of perforation).

3.1. Numerical modelling of the impact problem

The finite element code Abaqus Explicit v6.44 (HKS, 2003) has been used to simulate the impact cases. The adhesive layer slightly affects the degree of fragmentation of the ceramic material, and the transmission of the impulsive energy to the backing plate. A thin adhesive layer prevents fragmentation but reduces dissipation of the energy through plastic deformation of the metal back plate. Also adhesive materials with a mechanical impedance close to that of the ceramic helps to reduce fragmentation (Zaera et al., 2000; López-Puente et al., 2005). However the adhesive layer has been avoided in the numerical model in order to reduce the number of inputs of the network and to limit its predictive ability to the most influential parameters. Consequently, a unilateral contact condition has been defined between the ceramic tile and the metal plate because, as we have checked in preliminary studies, bilateral condition introduces too much stiffness in the armour.

Due to the high speed of the process, it has been considered as adiabatic. A parametric structured mesh (Fig. 4) was developed to easily generate the large number of geometries required for all the impact cases. 8-node trilinear displacement and temperature, reduced integration with hourglass control elements were employed in the mesh with a characteristic length $L_c = 1.5$ mm. The element includes the temperature as a degree of freedom to capture the thermal softening and the dilation. No boundary conditions were established due to the short duration of the process (maximum 150 μs) and an initial condition of velocity, v_i, in the impact direction was imposed to the nodes of the projectile.

The interactions between ceramic tile and metal backplate and between projectile and armour were modeled with the *general contact-kinematic contact algorithm* implemented in Abaqus Explicit (HKS, 2003). Since penetration is expected to occur between the projectile and the armour, a pure master–slave weighting was used in the interaction between both solids. The master surface being all the upper faces of the elements forming the armour and the slave surface, the projectile nodes. In this way, although certain elements of the head of the projectile and of the armour are deleted, the contact between the two solids was maintained throughout the penetration process. For the interaction between the ceramic tile and the metal backplate, as no penetration is expected, a balanced weighting was used.

3.1.1. Constitutive equations

For structural materials used in ballistic applications, elastic strains (and rates) are commonly very small compared to unity or to inelastic strains (and rates). So hypoelastic–plastic material models are employed in this work, allowing to assume the additive decomposition of the rate of deformation tensor (Nemat-Nasser, 1982; Khan and Huang, 1995).

For modelling the behaviour of metal alloys, a J_2 plasticity, with isotropic hardening constitutive law was adopted. To take into account the rate-dependent behaviour and the thermal softening by adiabatic heating that metals undergo in this kind of process, the hardening/softening Johnson–Cook law (Johnson and Cook, 1983) was employed. Table 1 shows the values of the parameters of the model for the metal alloys and their corresponding references. To model the erosion experimented by

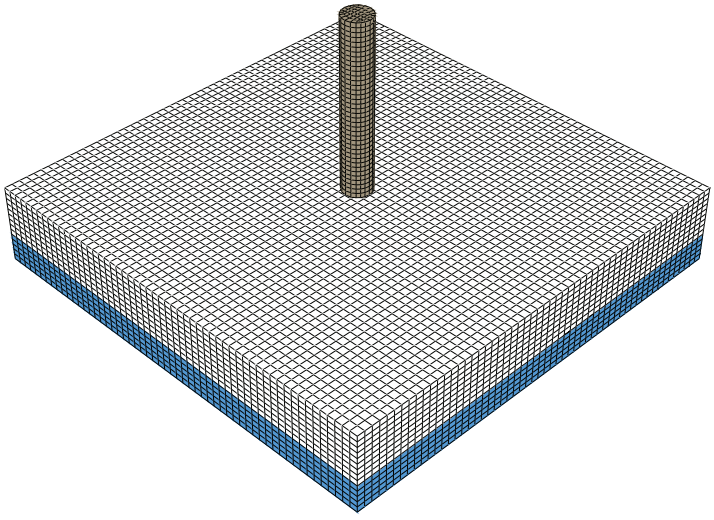

Fig. 4. Parametric mesh used in the simulations.

Table 1
Properties of metal alloys employed in the simulations (Johnson Cook parameters)

Parameter	Aluminium 6061 T6 (Dabboussi and Nemes, 2005)	AISI 4340 steel (Banerjee, 2007)	Mild steel (Myungsoo et al., 2005)	Tungsten alloy (Zhigang et al., 2001)
E (GPa)	73	208	200	345
ν	0.33	0.3	0.3	0.33
Density (kg/m^3)	2705	7850	7870	17,600
A (MPa)	335	1150	532	1093
B (MPa)	85	739	229	1270
n	0.11	0.26	0.3	0.42
C	0.012	0.014	0.027	0.0188
$\dot{\varepsilon}_0$ (s ^{1})	1	1	1	1
m	1	1.03	1	0.78
θ_0 (°C)	25	25	25	25
θ_m (°C)	600	1520	1520	1580
Specific heat (J kg ^{1} K ^{1})	963	500	481	134
Conductivity (W m ^{1} K ^{1})	170	44.5	44.5	45
Thermal exp. coef. (°C ^{1}) $\times$ 10 ^{5}	2.2	1.3	1.3	4.3
Quinney Taylor coefficient	0.7	0.8	0.85	0.7

the projectile and the metal backplate, a simple failure model based on the plastic equivalent strain has been adopted (*shear failure* in Abaqus Explicit), so that when ε_p reaches a critical value $\varepsilon_{failure}$, the element is deleted from the model. Certainly the element deletion technique causes an artificial loss of momentum in the system. However, the model reproduces with accuracy classical experimental results in the impact mechanics field, as will be shown in Section 3.1.2.

Constitutive equations to model the ceramic material behaviour against high velocity impact are not implemented in most of the commercial finite element codes, specifically in Abaqus Explicit (HKS, 2003). Although there are more complex constitutive relations to model the dynamic fragmentation undergone by the ceramic tile like that developed by Curran et al. (1993) or the Denoual–Hild model (Denoual and Hild, 2002), we propose a model that makes a simpler description of the fragmentation process and allows to achieve precise results in terms of the resistance of the ceramic to be penetrated and, consequently, in its behaviour against high-velocity impact. This model is based in the work of Cortés et al. (1992), which takes into account the progressive fragmentation of a monolithic intact ceramic material by means of a damage variable D varying in the range $[0,1]$ (intact-pulverized material). The model considers a Drucker-Prager law for the intact material and a pure frictional law for the pulverized material, defining the intermediate states as an average of both situations (Fig. 5). The yield function f is given by Eq. (14)

$$f = \sigma \quad (1 \quad D)(3\alpha p + \sigma_{0y}) \quad \mu p D, \tag{14}$$

where σ is the equivalent stress, p the hydrostatic pressure and 3α, σ_{0y}, μ material parameters. Cortés et al. (1992) proposed a law for the evolution of damage driven by the hydrostatic stress. In the modification proposed in this paper, the damage growth is driven by the maximum principal stress σ_1. Since hydrostatic stress is more appropriate as governing variable for void nucleation and growth processes in ductile materials, this modification was considered consistent with crack apparition and propagation phenomena in ceramic materials. Then the damage growth law is given by

$$\dot{D} = \dot{D}_0 \langle \sigma_1 \quad \sigma_0 \rangle. \tag{15}$$

$\dot{D}_0$ and σ_0 being material parameters. The maximum principal stress σ_1 is obtained with the expression

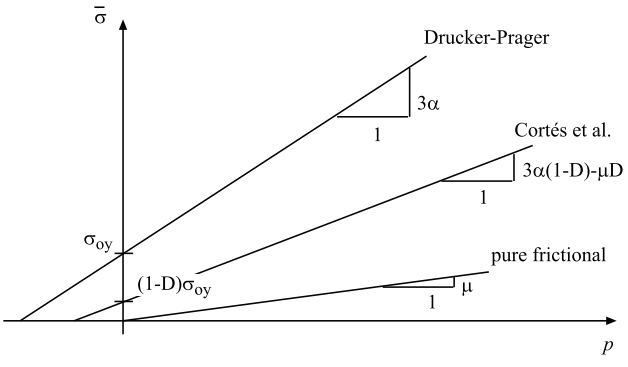

Fig. 5. Cortés et al. model (Cortés et al., 1992): influence of the pressure and the damage variable D in the yield function.

$$\sigma_1 = \quad p + \frac{2}{3}\sigma \cdot \cos\gamma, \tag{16}$$

where the Lode angle γ is defined by

$$\cos 3\gamma = \frac{3\sqrt{3}}{2}\frac{J_3}{\sqrt{J_2^3}}. \tag{17}$$

J_2 and J_3 being the second and third invariants of stress deviator.

The relation between stress and elastic strain is written as

$$\sigma^{\nabla} = C : d^{e} = C : (d \quad d^{p}), \tag{18}$$

σ^{∇} being an objective derivative of the Cauchy stress tensor, d and d^{p} the rate of deformation tensor and the rate of plastic deformation tensor, and C the linear isotropic elastic tensor, non dependent of damage, defined by

$$C = 2GI_{dev} + K1 \otimes 1, \tag{19}$$

where I_{dev} is the deviatoric fourth-order projection tensor, 1 is the second-order identity tensor, and G and K are the elastic constants

$$G = \frac{E}{2(1+v)}, \tag{20}$$

$$K = \frac{E}{3(1 \quad 2v)}. \tag{21}$$

For calculating the rate of plastic deformation a non-associative flow rule was chosen

$$d^{p} = \dot{\lambda}\frac{\partial \Psi}{\partial \sigma}, \tag{22}$$

where the plastic flow potential Ψ is formally analogous to the yield function (Eq. (14)) but with a lower pressure derivative what avoids an overestimation of the dilatancy effect of the fragmented ceramic material when inelastic deformations occur (Curran et al., 1993)

$$\Psi = \sigma \quad (1 \quad D)(3\alpha_{\psi} p + \Upsilon) \quad \mu_{\psi} pD, \tag{23}$$

where $\alpha_{\psi} = k\alpha$ and $\mu_{\psi} = k\mu$ (with $k < 1$). Υ is an irrelevant constant that disappears in the expression of the stress gradient of the plastic flow potential

$$\frac{\partial \Psi}{\partial \sigma} = \frac{3}{2}\frac{s}{\sigma} + \left[(1 \quad D)\alpha_{\psi} + \frac{\mu_{\psi} D}{3}\right]1. \tag{24}$$

The formulation of the model is completed by introducing the Kuhn–Tucker loading/unloading complementary conditions

$$\lambda \geqslant 0, \quad f \leqslant 0, \quad \lambda f = 0 \tag{25}$$

and the consistency condition

$$\lambda \dot{f} = 0. \tag{26}$$

The constitutive model was implemented in Abaqus Explicit code through a user subroutine, using a return mapping integration algorithm. The values of the parameters for the ceramics employed in the simulations (alumina and aluminum nitride) are shown in Table 2.

Table 2
Modified Cortés model: parameter values for alumina and aluminium nitride (Fernández Fdz, 2007)

Parameter	Alumina	Aluminum nitride
E (GPa)	378	310
v	0.22	0.21
σ_y (MPa)	240	230
Density (kg/m^3)	3810	3230
3α	0.65	0.785
σ_{0y} (MPa)	292	290
μ	0.21	0.1
$\dot{D}_0$ (Pa s) ^{1}	8×10^{3}	9×10^{2}
σ_0 (MPa)	240	230
k	0.7	0.65

Table 3
Armour thicknesses and impact velocities V_1 and V_2 for each impacted armour configuration (Den Reijer, 1991)

Alumina thickness (mm)	Aluminum thickness (mm)	V_1 (m/s)	V_2 (m/s)
8.1	6	815	916
8.1	8	995	1091

3.1.2. Validation of the numerical model

The model has been validated with some of the experimental results of Den Reijer (1991) for impacts on alumina–aluminum armours. This autor developed a flash radiography system to measure the position of the projectile and the armour during the process of penetration. The essays were carried out for two different configurations of the armour, having two impact velocities in each configuration, one, V_1 corresponding to projectile arrest and the other, V_2, corresponding to armour perforation. The essays are summarized in Table 3. Fig. 6 shows the position of the rear-end projectile and the maximum displacement of the armour for both, experimental and numerical results. The model predicts these variables with accuracy for both, complete perforation of the armour and projectile arrest. In Fig. 7 is shown the aluminium backplate after impact of one of the impacted armours (Table 3). One can see how the deformations predicted by the numerical simulation are in agree with the experimental results.

3.2. Numerical results postprocessing

To determine the residual velocity and residual mass of the projectile, once the calculations were carried out, we developed a post-processing application that determines these parameters from simulation output files following the next scheme:

- Reading from simulation output files: initial positions and final displacements of projectile nodes, connectivity matrix elements-nodes and the list of non-eroded elements of the projectile.

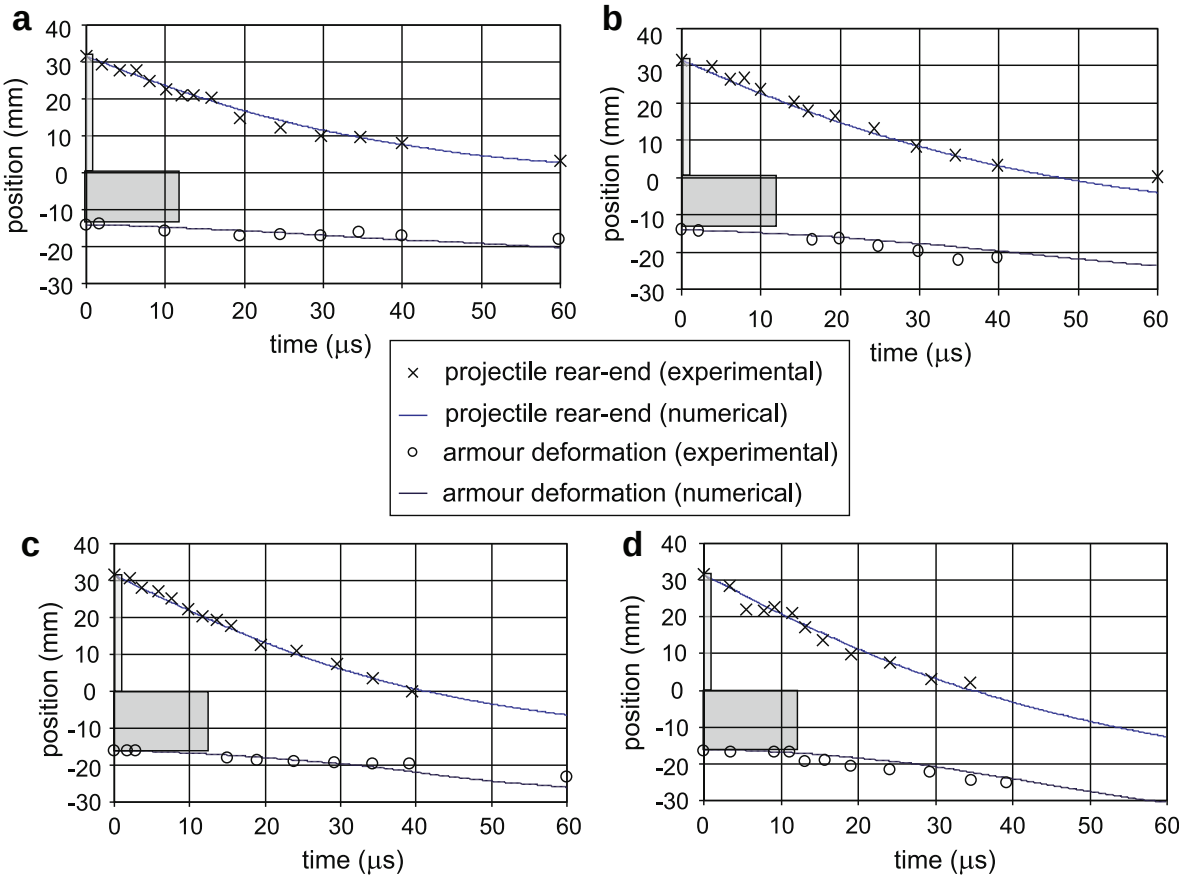

Fig. 6. Comparison between numerical and experimental position versus time curves of the rear end projectile and the maximum displacement of the armour for (a) 8.1 mm alumina backed by 6 mm aluminium, impact velocity $v = 815$ m/s, (b) 8.1 mm alumina backed by 6 mm aluminium, impact velocity $v = 916$ m/s, (c) 8.1 mm alumina backed by 8 mm aluminium, impact velocity $v = 995$ m/s, (d) 8.1 mm alumina backed by 8 mm aluminium, impact velocity $v = 1091$ m/s.

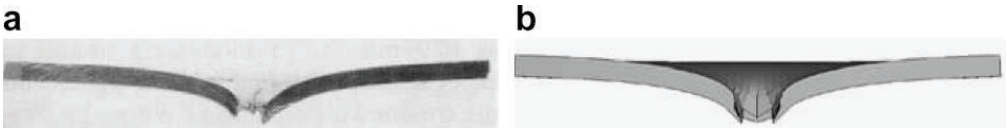

Fig. 7. 6 mm aluminium backplate of an alumina aluminium armour after impact with a steel projectile impacted at 916 m/s. (a) Experimental result (Den Reijer, 1991) and (b) numerical result.

- Calculation of final positions of projectile nodes.
- Mapping the non-eroded elements to their corresponding origin-centered regular hexahedron.
- Integration in this new domain, for each non-eroded-element, of mass and linear momentum by means of eight Gaussian points of integration.
- Sum of the mass and linear momentum for all non-eroded elements of the projectile.
- Calculate the averaged velocity of the projectile by dividing the total linear momentum by the total mass.

4. Multilayer perceptron development

For an impact case (or pattern) defined in the space of variability $\mathscr{R}$, the determination of the occurrence of perforation corresponds to a *pattern-recognition problem*. The network acts as a classifier deciding whether the pattern belongs to the class of armour perforation cases or the class of projectile arrest cases. The classification is done by means of two outputs given by the network, varying in a continuous range [0, 1], which represents the probability of belonging to both classes, these variables being complementary. This task is performed by one network (*MLP1*). The determination, in the case of perforation, of the residual mass and the residual velocity of the projectile is considered a *regression problem* in which the network predicts these variables as a function of the input pattern. A second network (*MLP2*) was developed to perform this task. Both Perceptrons were constructed with the neurocomputing code *NeuroSolutions for Excel* v4.21 (NDS, 2003). The development methodology in both cases consists of the following steps:

- Determine, from the variables defining the problem, the ones constituting the best inputs to form the input pattern **x**.
- Train the network by varying the number of neurons N_H in the hidden layer (a MLP with two hidden layers was tried in preliminary studies giving similar results to those found using a MLP with one hidden layer, and therefore the latter was employed).
- Test the best topology found in the training step.

Once the MLPs were tested (if the testing results are enough precise) they are used as a predictive tool and can be used to produce output data.

4.1. Determination of the optimal input variables

To identify the most influential variables in this problem is crucial, not only for the determination of the input variables of the network but to gain a good understanding of the physical phenomenon. To select these variables for the occurrence of perforation (pattern-recognition problem), we developed the following method, based on the distance of Mahalanobis, which reduces the classification error.

Let x_i be the input variable analysed; let x_i^{perf} and $\hat{x}_i^{\text{perf}}$ be its mean and standard deviation in the set of patterns corresponding to armour perforation; and let x_i^{par} and $\hat{x}_i^{\text{par}}$ be its mean and standard deviation in the set of patterns corresponding to projectile arrest. The relative distance between both means $\mathrm{d}x_i$ is defined as

$$\mathrm{d}x_i = 2\frac{|x_i^{\text{perf}} \quad x_i^{\text{par}}|}{x_i^{\text{perf}} + x_i^{\text{par}}}. \tag{27}$$

Defining the normalized standard deviation associated with the input variable x_i as

$$\hat{x}_i = \frac{\hat{x}_i^{\text{perf}} + \hat{x}_i^{\text{par}}}{x_i^{\text{perf}} + x_i^{\text{par}}}. \tag{28}$$

One can define an uncertainty parameter X_i associated to the input variable x_i by dividing Eq. (28) by Eq. (27)

$$X_i = \frac{\hat{x}_i}{d_{xi}}. \tag{29}$$

X_i can be used as an estimation of the classification error when a pattern is classified using the input variable x_i. Large values of X_i correspond to small distances between means and/or large standard deviations, x_i exhibiting then great uncertainty for

Table 4
Values of x_i^{perf}, x_i^{par}, $\hat{x}_i^{perf}$, $\hat{x}_i^{par}$, dx_i, $\hat{x}_i$ and the uncertainty parameter X_i for each variable x_i

x_i	x_i^{perf}	x_i^{par}	$\hat{x}_i^{perf}$	$\hat{x}_i^{par}$	dx_i	$\hat{x}_i$	X_i
L_p (m)	0.0370	0.0354	0.0115	0.0123	0.044	0.329	7.48
$\mathbf{D}_p$ (m)	0.0085	0.0073	0.0023	0.0024	0.152	0.294	**1.93**
$\mathbf{v}_i$ (m/s)	948	654	176	128	0.367	0.190	**0.52**
H_c (m)	0.0102	0.0110	0.0040	0.0045	0.095	0.407	4.28
H_m (m)	0.0061	0.0063	0.0027	0.0027	0.032	0.436	13.62
H_t (m)	0.0163	0.0172	0.0064	0.0057	0.054	0.360	6.67
$\mathbf{m}_i$ (g)	35.4	16.7	28.2	15.4	0.718	0.837	**1.16**
$\mathbf{L}_p/\mathbf{D}_p$	4.39	4.82	0.88	0.75	0.093	0.177	**1.90**
$\mathbf{L}_p/\mathbf{H}_t$	2.37	2.12	0.47	0.47	0.111	0.209	**1.88**
$\mathbf{L}_p/\mathbf{H}_c$	3.82	3.42	0.86	0.82	0.110	0.232	**2.11**
L_p/H_m	6.50	5.90	1.71	1.65	0.097	0.272	2.80

the prediction of the occurrence of armour perforation. Thus the variables x_i, having smaller values of X_i (D_p, v_i, m_i, L_p/D_p, L_p/H_t and L_p/H_c), have been selected as the inputs of the network *MLP1*, together with the material indentifiers for the projectile, backplate, and ceramic tile (see Table 4).

To determine the optimal input variables to obtain the residual mass and residual velocity of the projectile (regression problem), we performed a correlation analysis between possible inputs and these four output variables (the absolute values m_r, v_r and the corresponding values normalized by the initial velocity v_i and the initial mass m_i). Table 5 shows the regression coefficients R_{ij}^2 for the best fit found, linear or power, associated with the pair of variables (x_i, y_j). Due to the large differences in densities between steel and tungsten we have made the correlation analysis, separating the patterns by projectile material because it improves the value of R_{ij}^2. The best correlations are given for (v_i, v_r) and for (m_i, m_r), what is reasonable taking into account that the perforation process is momentum driven (Woodward, 1990). The quotients L_p/H_t, L_p/H_c and L_p/H_m show a better correlation with the normalized residual variables whereas H_t and H_c and H_m have no significant correlation with the residual velocity (absolute or normalized). It is worth also to note that projectile aspect ratio has a minimal influence in output variables. Viewing these results, we have maintained the same inputs employed in *MLP1* except the aspect ratio of the projectile, which was removed. We also included the normalized variables v_r/v_i and m_r/m_i in the output pattern because they were significatively correlated with the quotients L_p/H_t and L_p/H_c.

4.2. Training and testing of the networks

4.2.1. Training

The networks to be trained, *MLP1* and *MLP2*, are shown in Fig. 8. Linear functions were used as activation functions in the input layer. Hyperbolic tangent and logistic functions were used in the hidden and output layers having similar results so finally hyperbolic tangent was used in these layers. Since the learning rate ξ influences in the convergence rate of the learning process but not significatively in the final results (Rumelhart et al., 1986), the default values proposed by the neurocomputing code *NeuroSolutions for Excel* v4.21 (NDS, 2003) were used: $\xi = 1$ in the hidden layer and $\xi = 0.1$ in the output layer. 170, 15 and 15 impact cases were randomly chosen for the learning, cross-validation and test sets of patterns respectively. This operation was performed for each network. Both MLPs were trained varying the number of neurons in the hidden layer N_H to determine its optimum value. An initial estimate for N_H can be determined by $N_H = \sqrt{NM}$, N and M being the number of neurons in the input and output layer, respectively (Tarassenko, 1998). This formula leads to five hidden neurons for the first perceptron and seven hidden neurons for the second. However, different values of N_H were also tried: $N_{H1} = 4, 5, 6$ for *MLP1* and $N_{H2} = 6, 7, 8, 9$ for *MLP2*.

Table 5
Matrix of correlation coefficients R_{ij}^2 between input x_i and output y_j

	v_r	v_r/v_i	m_r	m_r/m_i
L_p	NV	4.5×10^{-2}/NV	0.75/0.8	2×10^{-2}/NV
$\mathbf{D}_p$	NV	3×10^{-2}/1.1×10^{-2}	**0.92/0.94**	0.12/4×10^{-2}
$\mathbf{v}_i$	**0.95/0.61**	0.42/0.44	NV/1.7×10^{-2}	3×10^{-2}/0.25
H_c	NV	1.4×10^{-2}/10^{-2}	0.48/0.45	2×10^{-2}/8×10^{-2}
H_m	NV	NV	0.41/0.51	7×10^{-2}/6×10^{-2}
H_t	NV	NV	0.51/0.52	4×10^{-2}/8×10^{-2}
$\mathbf{m}_i$	NV	NV	**0.98/0.98**	5×10^{-2}/1.8×10^{-2}
L_p/D_p	NV	NV	NV	8×10^{-2}/5×10^{-2}
$\mathbf{L}_p/\mathbf{H}_t$	NV	$\mathbf{5 \times 10^{-2}/4 \times 10^{-2}}$	NV	**0.47/0.31**
$\mathbf{L}_p/\mathbf{H}_c$	NV	$\mathbf{10^{-2}/4 \times 10^{-2}}$	NV	**0.17/0.36**
L_p/H_m	NV	NV	NV	0.28/0.33

Each element R_{ij}^2 is composed for the correlation coefficient when separating patterns with tungsten and steel projectiles, respectively $((R_{ij}^2)^{tungsten}/(R_{ij}^2)^{steel})$.
NV, negligible value ($<10^{-2}$).

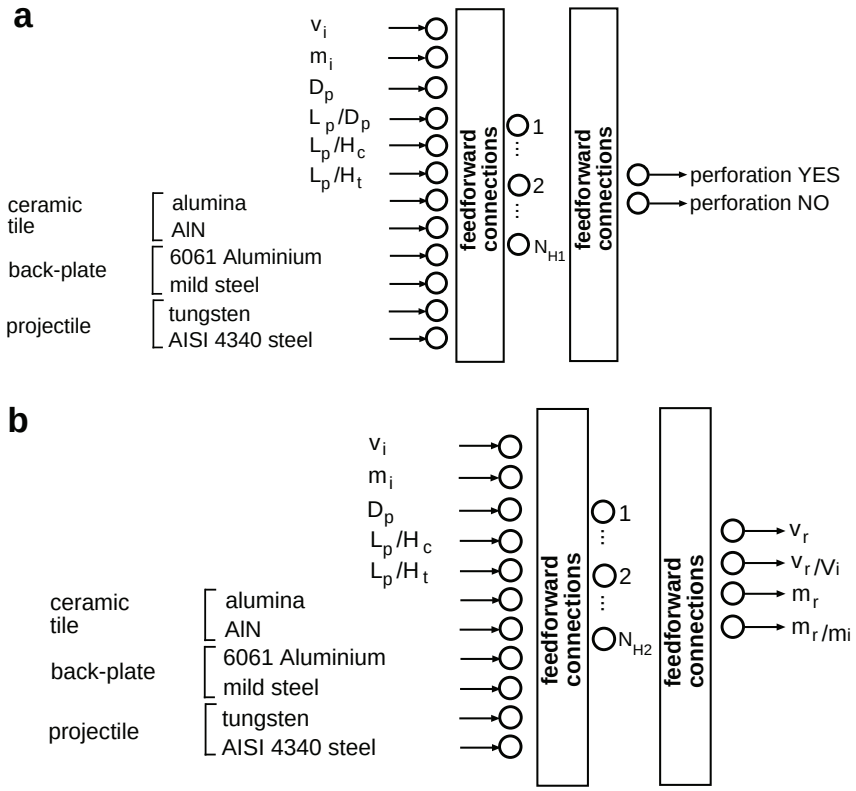

Fig. 8. (a) *MLP1* to predict the occurrence of perforation of the armour. (b) *MLP2* to predict the residual mass and velocity of the projectile.

As mentioned above, weights and thresholds are randomly initialized at the beginning of the training algorithm. This procedure, routine in network training, leads to a variability in the results found by the network that can be observed when two networks having the same topology, trained with the same data and the same algorithm, produce slightly different results. This variability is treated by generating a family of networks that is quite wide (50 networks in this case) for each topology, defined by N_H, with a different randomized value for the initial weights and thresholds. For each family, all of the networks are trained and it is chosen that one having the minimum value of the mean squared error $MSE^{\mathscr{L}}$ when the stop criterion is reached (the cross-validation error $MSE^{\mathscr{V}}$ reaches its minimum value). Table 6 shows these values for different N_H. Viewing these results, we chose $N_{H1} = 4$ and $N_{H2} = 8$.

4.2.2. Testing

Once the best topologies were determined, the MLPs were tested with the independent data of the testing sets of patterns. *MLP1* has correctly classified all the impact cases except for one pattern. For this pattern an output value for "PERFORATION YES" close to 1 was expected (corresponding to an armour perforation case), but *MLP1* gave "PERFORATION YES" = 0.29. This error is explained by the fact that this pattern corresponds to the tungsten projectile with the second minimum velocity (525 m/s) over the 200 impact cases considered. It is known that the network loses precision for patterns that contain values of the input variables close to the limits imposed in the definition of the problem (Bishop, 1995) (see expression (13)).

In the calculations of the residual variables, the results found during the test by *MLP2* were more precise for the normalized variables v_r/v_i and m_r/m_i than for the absolute values v_r and m_r. Therefore, normalized values were used to calculate the desired outputs. *MLP2* provided, for the residual velocity, an averaged relative error of $\overline{E}_{v_r} = 7.5\%$ and a maximum error $E^{max}_{v_r} = 13.9\%$. Only for one impact case of the testing set, did the network exceed this maximum value giving, for that case, an error $E^{*}_{v_r} = 44\%$. This large value can also be explained by the fact that, for this impact, the quotient V_r/V_i reaches an extreme value (Fig. 9).

Table 6
$MSE^{\mathscr{L}}$ for different values of N_H in both MLPs when training algorithm has converged (minimum $MSE^{\mathscr{V}}$)

MLP1		*MLP2*	
N_{H1}	$MSE^{\mathscr{L}}$	N_{H2}	$MSE^{\mathscr{L}}$
4	**0.0057**	6	0.011
5	0.0066	7	0.0083
6	0.0098	**8**	**0.0035**
		9	0.0048

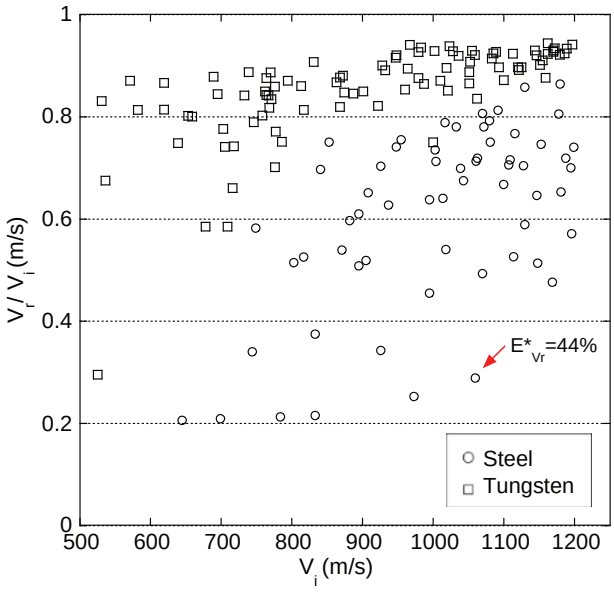

Fig. 9. v_r/v_i vs. v_i. for the 200 impact cases, separated by projectile material. Testing case in which *MLP2* has reached a large error (44%).

The results were significantly better in the calculation of the residual mass. *MLP2* provided an averaged relative error $\overline{E}_{m_r} = 2.9\%$ and a maximum error $E^{max}_{m_r} = 6.8\%$. These precise results were because of the high correlation between the output m_r and the inputs D_p and m_r (Table 5).

4.3. Results and discussion: employing MLPs as predictive tools

Once the networks are tested, they can be used to simulate the behaviour of ceramic–metal armours against high-velocity impact. The curves of probability of perforation, in order to determine the ballistic limit v_{50}, are one of the classical ways to study this problem. *MLP1* can be used to reproduce these curves taking into account that the output "PERFORATION YES" varying in the range [0,1] is an estimate of the probability of perforation (Bishop, 1995) for a system projectile-armour. Fig. 10a shows these probability curves resulting with *MLP1* for three different armours built up with a tile of alumina backed with a plate of aluminum 6061-T6 of different thicknesses: 8.1 mm alumina/4 mm aluminum, 8.1 mm alumina/6 mm

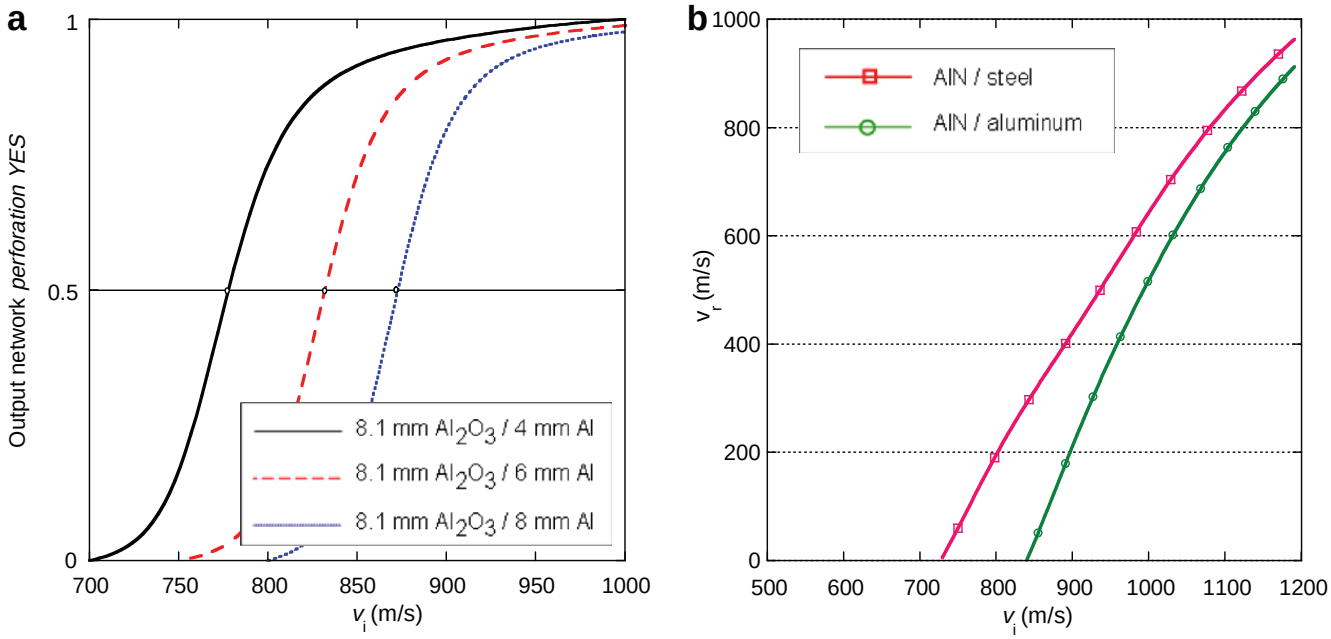

Fig. 10. (a) Curves of probability of perforation for three bi layered armours alumina/aluminium of different thicknesses: 8.1 mm alumina/4 mm aluminum, 8.1 mm alumina/6 mm aluminum and 8.1 mm alumina/8 mm aluminum. (b) Curves of residual velocity vs. impact velocity for two bi layered armours having the same areal density ($A_D = 50$ kg/m^2).

Table 7
Values for v_{50} estimated from the experimental results (Den Reijer, 1991), values found by *MLP1* and *MLP1* error

	Den Reijer (1991)	*MLP1*	Error (%)
v_{50} (8.1 mm Al_2O_3/4 mm Al)	807	778	3.6
v_{50} (8.1 mm Al_2O_3/6 mm Al)	865	832	3.8
v_{50} (8.1 mm Al_2O_3/8 mm Al)	1093	872	16

aluminum and 8.1 mm alumina/8 mm aluminum. The armours were impacted with a cylindrical hard-steel projectile of 31.5 mm in length and 6 mm in diameter. The ballistic limits v_{50} found with the curves are also shown. Table 7 shows the experimental results of Den Reijer (1991) and the error of *MLP1*. The predictions for the thicknesses of 8.1 mm alumina/4 mm aluminum and 8.1 mm alumina/6 mm aluminum proved to be very precise, for the thickness 8.1 mm alumina/8 mm aluminum the error increases. This also can be explained, as in the testing cases where the error was important, by looking at the values of the variables that define this impact case. While for the first two cases $H_c = 2H_m$ and $H_c = 1.33H_m$ in the third case $H_c = H_m$. This condition corresponds to an extreme value in the definition of the impact cases used to train and test the networks (expression (13)). Thus, when the impact case is defined by means of variables whose values are well inside of the range defined by expression (13), *MLP1* makes precise predictions.

Other important tools in the study of the behaviour of ceramic–metal armours are the curves of residual velocity versus impact velocity. These curves can be simulated from the residual velocity determined by *MLP2*. To illustrate the performance of the network, Fig. 10b shows the curves for two armours combining aluminium nitride with mild steel and aluminium 6061-T6, impacted with a cylindrical hard-steel projectile of 31.5 mm in length and 6 mm in diameter. The areal density for both armours is $A_D = 50\ \mathrm{kg/m^2}$. Once the networks have been developed, these kind of curves, as well as the probability perforation ones, can be obtained easily with low cost and in a short time.

4.4. Conclusions

From the testing of the neural networks and the results presented and discussed, the main conclusions are:

- The MLP predicts either the impact-body arrest or the target perforation for a wide range of impact cases, including different geometries and materials for the impacting body and the target, and for different impact velocities.
- In case of target perforation, the MLP predicts the residual velocity of the impacting body with a mean error of 7.5% and a maximum error of 13.9% and the residual mass with a mean error of 2.9% and a maximum error of 6.8%.
- When the network is used to predict the impact behaviour of a projectile/armour system, the values of the input data that define the system should not be close to the limit values used to define the cases used to train the network.
- Once the MLPs are trained and tested, real-time results are given. Solving 1000 impact cases has an approximate computational cost of 1 second.
- For the selection of the most suitable input variables for the MLP, the proposed methodology permits us to determine which variables facilitate the classification and regression tasks performed by the network.

In view of the above, we conclude that the MLP developed here offers remarkable prediction ability of the impact behaviour of lightweight ceramic–metal armours and therefore it constitutes a complementary methodology to the traditional ones. This tool can be used to develop common curves in ballistics, such as the probability of perforation curves and the residual-velocity vs. impact-velocity curves.

Acknowledgements

The authors are indebted to the Comunidad Autónoma de Madrid and to the University Carlos III of Madrid for the financial support of this work (CCG07-UC3M/DPI-3395).

References

Adeli, H., Yeh, C., 1989. Perceptron learning in engineering design. Microcomp. Civil Eng. 4, 247 256.
Banerjee, B., 2007. The mechanical threshold stress model for various tempers of AISI 4340 steel. Int. J. Solids Struct. 44 (3 4), 834 859.
Bishop, C., 1995. Neural Networks for Pattern Recognition. Oxford University Press, Oxford.
Chandrashekhara, K., Okafor, A., Jiang, Y., 1998. Estimation of contact force on composite plates using impact induced strain and neural networks. Composites B 29 (4), 363 370.
Chocron Benloulo, I., Sánchez Gálvez, V., 1998. A new analytical model to simulate impact onto ceramic/composite armors. Int. J. Impact Eng. 21 (6), 461 471.
Cortés, R., Navarro, C., Martínez, M.A., Rodríguez, J., Sánchez Gálvez, V., 1992. Numerical modelling of normal impact on ceramic composite armours. Int. J. Impact. Eng. 12, 639 651.
Cottrell, M., Yu, J., Owen, D., 2003. The adaptive and erosive numerical modelling of confined boron carbide subjected to large scale dynamic loadings with element conversion to undeformable meshless particles. Int. J. Impact Eng. 28 (9), 1017 1035.
Curran, D., Seaman, L., Cooper, T., Shockey, D., 1993. Micromechanical model for comminution and granular flow of brittle material under high strain rate application to penetration of ceramic targets. Int. J. Impact Eng. 13 (1), 53 83.
Dabboussi, W., Nemes, J.A., 2005. Modeling of ductile fracture using the dynamic punch test. Int. J. Mech. Sci. 47 (8), 1282 1299.

Denoual, C., Hild, F., 2002. Dynamic fragmentation of brittle solids: a multi scale model. Eur. J. Mech. A 21, 105 120.
Den Reijer, P. 1991. Impact on ceramic faced armour. Ph.D. Thesis, Delf University of Technology.
El Kadi, H., 2006. Modeling the mechanical behavior of fiber reinforced polymeric composite materials using artificial neural networks a review. Compos. Struct. 73 (1), 1 23.
Fernández Fdz, D. 2007. Desarrollo de una nueva herramienta basada en redes neuronales para el diseño de protecciones ligeras cerámica metal frente a impacto de alta velocidad. Ph.D. Thesis, University Carlos III of Madrid.
Florence, A., 1969. Interaction of Projectiles and Composite Armour. Part II. Stanford Research Institute, Menlo Park, CA,.
Hetherington, J. 1994. The protection and mobility of armoured fighting vehicles, Ph.D. Thesis, RMCS Shrivenham UK.
HKS, 2003. Abaqus Explicit v6.4 User's Manual, version 6.4 Edition, ABAQUS Inc., Richmond, USA.
Hohler, V., Weber, K., Tham, R., James, B., Barker, A., Pickup, I., 2001. Comparative analysis of oblique impact on ceramic composite systems. Int. J. Impact Eng. 26 (1 10), 333 344.
Ince, R., 2004. Prediction of fracture parameters of concrete by artificial neural networks. Eng. Fract. Mech. 71 (15), 2143 2159.
Johnson, G.R., Cook, W.H. 1983. A constitutive model and data for metals subjected to large strains, high strain rates, and temperatures. In: Proc. 7th Int. Symp. Ballistics, The Hague, The Nederlands, pp. 1 7.
Khan, A., Huang, S., 1995. Continuum Theory of Plasticity. Wiley, New York.
Liu, S., Huang, J., Sung, J., Lee, C., 2002. Detection of cracks using neural networks and computational mechanics. Comput. Meth. Appl. Mech. Eng. 191 (25 26), 2831 2845.
Liu, L., Zhang, Q., Zhai, P., 2003. The optimization design of metal/ceramic fgm armor with neural net and conjugate gradient method. Mater. Sci. Forum 423 425, 791 796.
López Puente, J., Arias, A., Zaera, R., Navarro, C., 2005. The effect of the thickness of the adhesive layer on the ballistic limit of ceramic/metal armours. An experimental and numerical study. Int. J. Impact Eng. 32 (1 4), 321 336.
Myungsoo, P., Jeonghoon, Y., Dong Teak, C., 2005. An optimization of a multi layered plate under ballistic impact. Int. J. Solids Struct. 42, 123 137.
NDS, 2003. NeuroSolutions for Excel v4.21. User's Manual, version 4.21 Edition. NeuroDimension Inc., Gainesville, USA.
Nemat Nasser, S., 1982. On finite deformation elastoplasticity. Int. J. Solids Struct. 18, 857 872.
Remennikov, R.T., Rose, A.M., 2007. Predicting the effectiveness of blast wall barriers using neural networks. Int. J. Impact Eng. 34 (12), 1907 1923.
Rumelhart, D., Hinton, G., Williams, R., 1986. Learning representations by back propagating errors. Nature 323, 533 536.
Shokrieh, M., Javadpour, G., 2008. Penetration analysis of a projectile in ceramic composite armor. Compos. Struct. 82 (2), 269 276.
Tarassenko, L., 1998. A Guide to Neural Computing Applications. Arnold/NCAF, London.
Waszczyszyn, Z., Pabisek, E., 1999. Hybrid nn/fem analysis of the elastoplastic plane stress problem. Comput. Assisted Mech. Eng. Sci. 6, 177 188.
Waszczyszyn, Z., Ziemianski, L., 2001. Neural networks in mechanics of structures and materials new results and prospects of applications. Comput. Struct. 79 (22 25), 2261 2276.
Wilkins, M., 1978. Mechanics of penetration and perforation. Int. J. Impact Eng. 16, 793 807.
Woodward, R., 1990. A simple one dimensional approach to modelling ceramic composite armour defeat. Int. J. Impact Eng. 9 (4), 455 474.
Zaera, R., Sánchez Gálvez, V., 1998. Analytical modelling of normal and oblique ballistic impact on ceramic/metal lightweight armours. Int. J. Impact Eng. 21 (3), 133 148.
Zaera, R., Sánchez Sáez, S., Pérez Castellanos, J.L., Navarro, C., 2000. Modelling of the adhesive layer in mixed ceramic/metal armours subjected to impact. Composites A 31 (3), 823 833.
Zhigang, W., Jilin, Y., Jianrong, L., Yongchi, L., Shisheng, H., 2001. Influence of stress condition on adiabatic shear localization of tungsten heavy alloys. Int. J. Impact Eng. 26, 843 852.